Corrosion Protection of AS21 Alloy by Coatings Containing Mg/Al Hydrotalcites Impregnated with the Organic Corrosion Inhibitor 2-mercaptobenzimidazole

E. F. Hernández Molina[1], A. Espinoza Vázquez[1,2,], F. J. Rodríguez Gómez[1], I. A. Figueroa[2*],
G. E. Negrón Silva[3], D. Ángeles-Beltrán[3].*

[1] Departamento de Ingeniería Metalúrgica, Facultad de Química, Universidad Nacional Autónoma de México, Ciudad de México, 04510, México
[2] Instituto de Investigaciones en Materiales, Universidad Nacional Autónoma de México, Circuito Exterior S/N, Cd. Universitaria, Coyoacán, Ciudad de México, 04360, México
[3] Departamento de Ciencias Básicas, Universidad Autónoma Metropolitana-Azcapotzalco,
Av. San Pablo No. 180, Ciudad de México, 02200, México
[*]E-mail: arasv_21@yahoo.com.mx, iafigueroa@unam.mx

This work provides an affordable strategy to enhance the corrosion resistance of hydrotalcite coating by chemical modification of the coating with 2-mercaptobenzimidazole. The corrosion protection of the AS21 alloy immersed in Hank's solution is described by means of coatings containing Mg/Al hydrotalcites impregnated with the organic corrosion inhibitor 2-mercaptobenzimidazole (HT-2-MBI). The effect of the coating concentration on the efficiency of corrosion inhibition was determined using the techniques of electrochemical impedance spectroscopy and polarization curves. A maximum efficiency of 92% was reached after 0.5 hours and 75% in a period of 102 hours.

Keywords: Hydrotalcites, 2-MBI, AS21 alloy, inhibitor, EIS.

1. INTRODUCTION

A very light metallic material in comparison to steel that has raised interest in recent years due to its uses in medicine is magnesium and its alloys [1]. Magnesium is considered in biodegradable orthopedic implants [2] for bone fracture fixation; however, as it undergoes a rapid corrosion process [3], this metal does not provide long-term mechanical support for the healing of fractures [4].

Nowadays, stents, bone plates and artificial limbs made from magnesium alloys (AZ31 [5] and AZ91 (Mg-Al-Zn) for use in patients, which have an elastic module of 45Gpa and a traction resistance of 200 MPa [6], which makes them resistant materials.

Recently, it has been reported that patients with this type of implant show subcutaneous gas cavities caused by the corrosion of the alloys used, which is why it is necessary to propose the use of coatings to inhibit corrosion [7]. It has been demonstrated that some coatings increase the corrosion resistance this kinds of alloys with biomedical applications [8], but they are only effective in short exposure periods.

A magnesium alloy available since 1970, the series AS (Mg-Al-Si) is commercially exploited on a large scale for use in the rear engine in several models of the Volkswagen Beetle automobile as a replacement for gray cast iron [9]. It is important to mention that its mechanical properties (tensile strength of 240MPa and yield strength of 130 MPa) are similar to those of the AZ91 alloy.

On the other hand, hydrotalcite is a mesoporous material with a similar structure to that of brucite $Mg(OH)_2$, in which magnesium is octahedrally coordinated to six hydroxyl groups, which, sharing their edges, form bidimensional layers. If the Mg^{+2} cations are partially replaced by a trivalent metallic ion as the Al^{3+}, the layer set acquires a positive residual charge, which is compensated by means of the alternation of anions in A^{m-} and water molecules in the inter-layer region expressed as $[Mg^{2+}_{1-x}Al^{3+}_x(OH)_2]^{x+}(A^{m-})_{x/m}\cdot nH_2O$. Hydrotalcites have been used in the synthesis of a great variety of coatings that have been shown to be useful as corrosion inhibitors [10-20].

The heterocyclic compound 2-mercaptobenzimidazole (2-MBI) is an efficient organic inhibitor of acid corrosion in API 5L X52 steel immersed in aqueous solutions of sulfuric acid and hydrochloric acid [21-23].
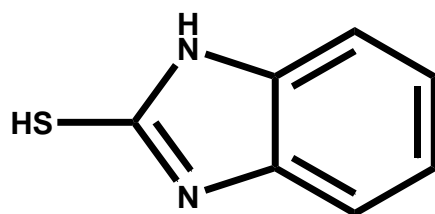

Figure 1. Chemical structure of 2-MBI

The aim of this work is to prepare the hydrotalcite (HT) and hydrotalcite impregnated with 2-mercaptobenzimidazole (HT-2-MBI) coatings and evaluate them as corrosion inhibitors of the AS21 alloy immersed in a physiological medium, as a Hank's solution.

2. EXPERIMENTAL METHODOLOGY

2.1. Preparation of hydrotalcites and impregnation with 2-MBI

To obtain the mesoporous material (hydrotalcite, HT), the methodology used by Sato and Reichle [24, 25] (supporting information) was followed. To 40 ml of the obtained gel, different concentrations

(50, 100 and 200 ppm) of 2-mercaptobenzimidazole (2-MBI) dissolved in ethyl alcohol were added. Afterwards, the gel with the inhibitor was put in agitation for 24 hours at room temperature.

2.2 Coating of AS21 alloy

Plates of 5mm x 20mm x 30mm of the AS21 alloy were cut, the nominal composition of which is Al: 2.20, Si: 0.98, Zn: <0.01, Mn: 0.16, Fe: <0.01, Cu: <0.001, Be: <0.001. The plates were produced by die-casting [26] and were sanded with silicon carbide abrasive papers of grit sizes 200, 320, 480, 600, 900 and 1200. Afterwards, alumina (Al_2O_3) of 0.1µm was used as an abrasive and degreasing was performed with ethyl alcohol at 98% in a Cristófoli Ultron 2 ultrasonic bath for 30 minutes.

The plates were coated when they were immersed in the hydrotalcite gel (HT) and in a suspension (HT-2-MBI) for 30 minutes at a temperature of $77 \pm 3°C$.

2.3 Electrochemical evaluation

2.3.1 Open Circuit Potential (OCP)

Before the electrochemical impedance test, the potential was stabilized for 1800 seconds to guarantee its previous stationary state.

2.3.2 Electrochemical Impedance Spectroscopy (EIS)

The AS21 plates with the HT and HT-2-MBI coatings immersed in a Hank's solution as physiological medium at a pH = 7.6 were analyzed by electrochemical impedance spectroscopy (EIS) with an amplitude of ±10 mV during a frequency interval (100 kHz to 0.1 Hz). Three electrodes made up the electrochemical cell: the working electrode (magnesium AS21 with an exposed area of 1 cm²), a saturated Ag/AgCl reference electrode, and a graphite counter electrode.

2.3.3 Polarization curves (PC)

The AS21 plates without a coating (Blank) and with 2-MBI (100 ppm), HT and HT-2MBI (100 ppm) coatings immersed in Hank's solution were evaluated by polarization curves from -50 mV to 900 mV at a rate of 60 mV/s. The same arrangement was used as in section 2.3.2 for the electrochemical cell and they were connected to a Gill AC potentiostat. The EC-Lab analysis was used for data interpretation.

2.3.4. HT-2-MBI coating persistence

A concentration of 100 ppm of HT-2-MBI was determined making measurements of EIS every 6 hours over the course of a week.

2.4. HT-2-MBI coating characterization

The AS21 alloy coated with HT-2-MBI (50, 100 and 200 ppm) was immersed in 100 mL of Hank's solution for 4 hours. Afterwards, the material was washed with distilled water and dried, and then the surface was analyzed by means of Scanning Electron Microscopy (SEM) using a Carl-Zeiss SUPRA 55 VP at 10 kV microscope, with a secondary electron detector.

3. RESULTS

3.1 Effect of the coating with the 2-MBI concentration with HTs by means of EIS

Figure 2 shows the Nyquist diagram of the AS21 alloy coated with HT-2-MBI. In the literature, it has been reported that the high frequency region of the impedance spectra corresponds to the properties of the coating, while the low frequency region is attributed to the properties of the double electric layer (C_{dl}). The pure AS21 alloy shows a time constant that indicates that the system is controlled by the charge transfer resistance, reaching a value of ~490 Ω cm^2 [27]. On the other hand, when the AS21 alloy coated with HT is immersed in a Hank's solution, a slight increase in the Z_{real} value is observed in comparison to the one without a coating, which is attributed to the fact that the hydrotalcite is working as a barrier to decrease the corrosion process.
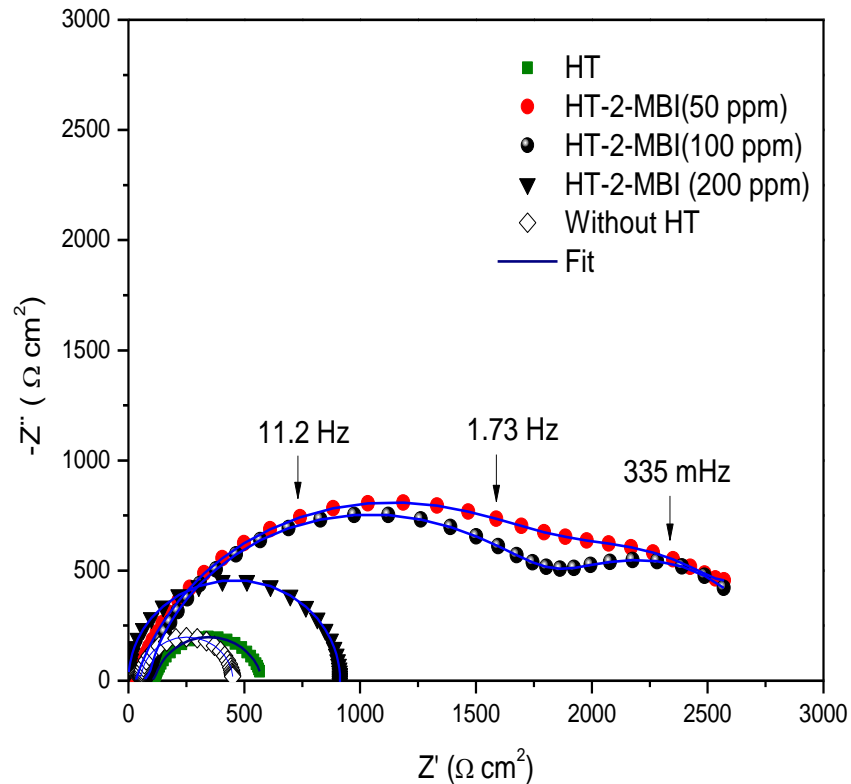

Figure 2. Nyquist diagram of the AS21 alloy with and without a coating (HT and HT-2-MBI) immersed in Hank's solution

However, in the AS21 alloy with the HT-2-MBI coating at different concentrations of 2-mercaptobenzimidazole, it can be observed that the semicircles are depressed, so two time constants are proposed: one attributed to the charge transference resistance and the other to the coating of the HT-2-MBI [28-30]. For the HT-2-MBI (100 ppm), a maximum value of Z_{real} (~2826.2 Ω cm²) was observed, and it was considered the best coating.

The equivalent circuits presented in Figure 3 were used to model the electrochemical behavior of the samples prepared without HT (circuit A) and with HT-2-MBI (circuit B). Where R_s is the solution resistance, R_F and Q_F are due to the conductivity in the coating and are described as a resistance net to the electrolytes and to the constant phase element of the film [31], respectively. R_{ct} and C_{dl} represent the charge transference resistance and the double layer capacitance.
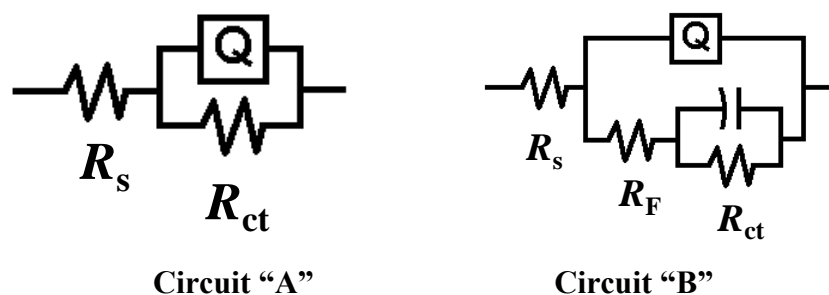

Circuit "A"   Circuit "B"

Figure 3. Equivalent electric circuits

The constant phase element (Q o CPE) of the impedance can be calculated thus:
$$Z_{CPE} = [Y_0 \, (j\omega)^n]^{-1} \tag{1}$$

Where Y_O is the CPE constant, n is the phase shift, j is the imaginary unit and ω is the angular frequency. According to the values of n, CPE can describe as the ideal condenser ($n = 1$), resistance ($n = 0$), inductance ($n = -1$) and Warburg impedance ($n = 0.5$).

The coating efficiency (η) is given by equation 2 [32, 33]:
$$\eta(\%) = \frac{\left(\frac{1}{R_{ct}}\right)HT - \left(\frac{1}{R_{ct}}\right)HT-2MBI}{\left(\frac{1}{R_{ct}}\right)HT} x100 \tag{2}$$

Where $1/R_{ct}$ HT is the charge transference resistance of the hydrotalcite without inhibitor and $1/R_{ct}$ HT-2-MBI is with inhibitor.

According to the values obtained from the simulation with electric circuits, it was observed that the hydrotalcite coating on the metallic surface decreased the corrosion process as the total resistance increased (Table 1). On the other hand, in the HT-2-MBI coating it was observed that the total resistance increased, so it can be concluded that there is a synergic effect between the mesoporous material and the 2-MBI. Consequently, the capacitance of the electrochemical double layer decreases because of the increase of the corrosion inhibition of the AS21 alloy. This decrease of the C_{dl} value is related to the increase in the protective layer with the thickness or decrease of the local dielectric constant [34]. It is

also shown that the capacitance C_F decreases with the concentration of 2-MBI of the coating (HT-2-MBI), which reached values of approximately 10 μFcm^{-2}, corresponding to the contribution of a very thin layer [32].

Table 1. Electrochemical parameters of the AS21 alloy of HT and HT-2-MBI immersed in Hank's solution

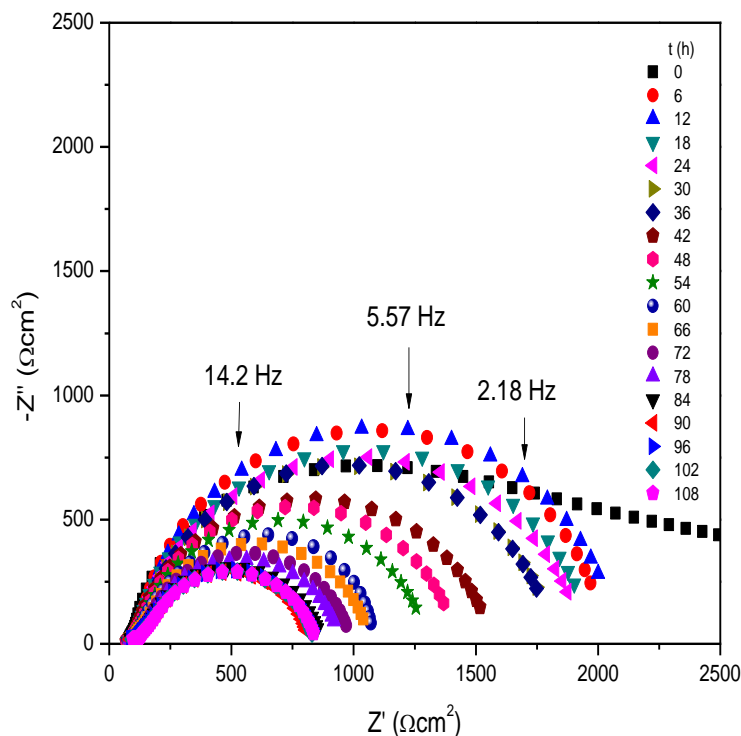| $C_{2\text{-MBI}}$ (ppm)	R_s (Ω cm²)	R_{ct} (Ω cm²)	n	C_{dl} (μF/cm²)	R_F (Ω cm²)	C_F (μF/cm²)	R_{total} (Ω cm²)	η (%)
0	27.2	209.2	0.7	1.5580	209.6	15.4	418.8	-
50	31.3	2166.0	0.8	0.7333	637.0	8.1	2803.0	85.0
100	74.7	1982.0	0.8	0.8820	876.4	1.0	2826.2	85.1
200	31.6	915.3	0.9	0.0300	154.6	1.5	1069.9	77.1

3.3. HT-2-MBI (100 ppm) coating persistence

Figure 4. Nyquist diagram of the AS21 alloy with HT-2-MBI (100 ppm) immersed in Hank's solution at different times

After performing the evaluation with the HT and HT-2-MBI, the coating containing the concentration of 100 ppm of 2-MBI was selected to observe the variation of the charge transference resistance and capacitance of the electrochemical double layer in the function of the immersion time.

It was observed that the Nyquist diagram in Figure 4 has two coupled time constants—one related to the charge transference and the other to the HT-2-MBI coating resistance. In general, it was observed that there was a gradual decrease (values of Z') as the immersion time increased, as a result of the desorption of 2-MBI in the hydrotalcite structure [33].

Table 2 summarizes the electrochemical parameters obtained after performing the corresponding adjustment with the electric circuit. It was observed that the values of R_{ct} with respect to the immersion time decreased gradually as the exposure time of the metallic surface with HT-2-MBI increased.

On the other hand, the value of R_F also presented a decrease after 6 hours of immersion, remaining practically constant at a longer immersion time. This is attributed to the fact that the coating is desorbing and increases its dissolution speed as the time increases [35].

Table 2. Electrochemical parameters of the AS21 alloy with HT-2-MBI (100 ppm) for different immersion times

t (h)	R_s (Ω cm^2)	n	R_{ct} (Ω cm^2)	C_{dl} (μF/cm^2)	R_F (Ω cm^2)	C_F (μF/cm^2)	R_{total} (Ω cm^2)	η (%)
Blank	27.2	0.7	209.2	1.55	209.6	15.4	418.8	-
0.5	74.5	0.8	1982	0.00	776.9	13.0	2758.9	92.4
6	78.62	0.8	1903	4.23	134.6	5.2	2037.6	89.7
12	81.71	0.8	1942	4.52	149.9	5.6	2091.9	90.0
18	81.71	0.8	1830	4.69	138.7	5.6	1968.7	89.4
24	82.00	0.7	1839	4.92	135.7	5.7	1974.7	89.4
30	82.79	0.7	1706	5.52	137.7	6.1	1843.7	88.7
36	71.25	0.7	1729	5.71	129.7	6.7	1858.7	88.7
42	67.77	0.7	1449	6.59	128.9	6.2	1577.9	86.7
48	68.27	0.7	1381	6.84	126.3	7.6	1507.3	86.1
54	72.85	0.7	1110	8.80	129.9	7.7	1239.9	83.1
60	73.54	0.7	972.3	9.49	124.5	4.6	1096.8	80.9
66	75.69	0.7	914.8	10.50	125.8	5.5	1040.6	79.9
72	77.59	0.6	844.8	11.50	122.2	10.1	967	78.4
78	80.53	0.6	786.9	12.60	119.1	10.6	906	76.9
84	80.91	0.6	729.0	12.90	114.1	13.7	843.1	75.2
90	83.77	0.6	640.7	14.50	122	12.0	762.7	72.6
96	83.77	0.6	693.3	13.50	121.4	16.9	814.7	74.3
102	88.28	0.6	679.5	13.70	114.6	12.6	794.1	73.7

However, in Figure 5 the behavior of the inhibition efficiency values for the different times is shown, where it was observed that the η remained with an acceptable effectiveness ($\eta > 80\%$), which suggests that the 2-MBI is still adsorbed in the hydrotalcite crystalline net. On the other hand, when the time increased, a process of desorption of the HT-2-MBI occurred, which involves an interchange of water molecules for the ones of the coating, producing a loss in its effectiveness [36].
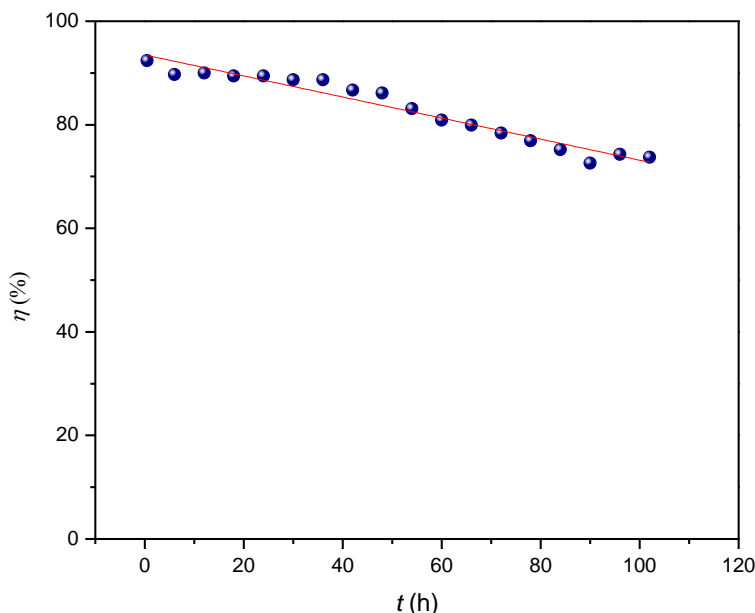
Figure 5. Variation of the inhibition efficiency of the HT-2-MBI (100 ppm) coating in the function of the immersion time

3.4. Polarization curves

Table 3 shows the electrochemical parameters obtained by means of polarization curves, as current density (i_{corr}), corrosion potential (E_{corr}), anodic and cathodic pendants (b_a and b_c) and inhibition efficiency calculated with equation 3.

The behavior observed in Figure 6 by means of the polarization curves of the metal with the inhibitor applied in situ (2-MBI) verifies a slightly lower current density compared to the pure metal. It is important to mention that, in the anodic current, a mechanism involving the positive ion Mg^{2+} governs; the pH of the solution remained in 8.1, promoting the following reaction mechanism [37]:

$$Mg \rightarrow Mg^{2+} + 2e^- \qquad\qquad\qquad \text{reaction 1}$$
$$Mg^{2+} + 2OH^- \rightarrow Mg(OH)_2 \qquad\qquad\qquad \text{reaction 2}$$

For the case of the AS21 surface with HT coating, the curve is almost identical to the one produced by the pure metal AS21 (Blank), hence, the i_{corr} is alike in magnitude. However, the anodic polarization curve of the sample coated with HT-2-MBI (100 ppm) presented a passive and not stable region, where the rupture potential appears until 689 mV. This is attributed to the fact that these samples show a higher corrosion potential and lower current density (the film has integrity to retard uniform corrosion), and in the passivation zone there is a nucleus of pitting in the Mg substrate.
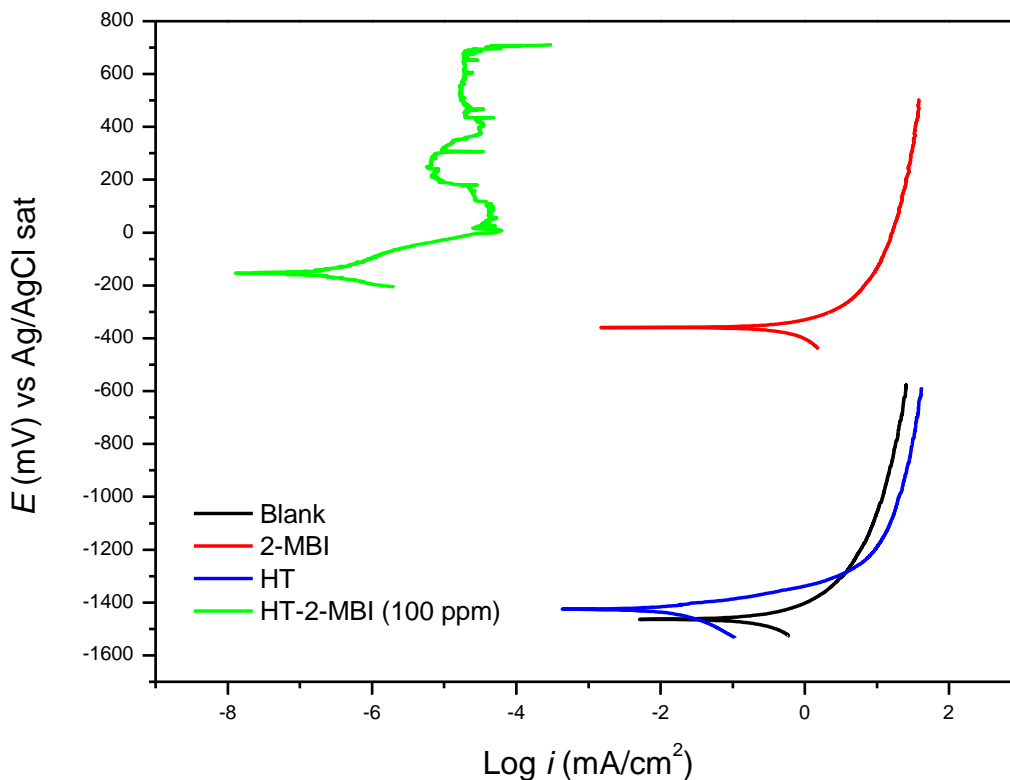
Figure 6. Polarization curves without coating (Blank), 2-MBI, HT and HT-2-MBI in AS21 alloy immersed in Hank's solution

On the other hand, the HT-2-MBI (100 ppm) coating showed a lower corrosion rate than the one without a coating. However, when only the 2-MBI and/or HT were evaluated on the metallic surface, similar behaviors were observed. This is attributed to the fact that, when isolated, they do not have an effect of decreasing the corrosion process. However, a synergic effect between the coating composed of the hydrotalcite and the 2-MBI as corrosion inhibitor was observed as it moved more to the left. From Table 3, some preliminary observations can be made, as there is a highl curve zone associated with an ohmic control. Further, the increase of the anodic current causes the formation of increasing amounts of Mg^{2+}, which match with the weight loss through the anodic polarization curve.

Table 3. Electrochemical parameters obtained by means of polarization curves

Conditions	b_a (mV/dec)	E_{corr} (mV vs Ag/AgCl)	i_{corr} (mA/cm²)	Corrosion Rate (mpy)
Blank	206	-1476	0.50	449.4
2-MBI (100ppm)	62	-487	0.10	107.3
HT	67	-1484	0.02	17.2
HT-2-MBI (100ppm)	69	-156	8.12×10^{-7}	7.2×10^{-4}

3.5 Superficial morphology

To corroborate the corrosion inhibition of the HT-2-MBI coating at different concentrations (50, 100 and 200 ppm of 2-MBI), the micrographics of the AS21 alloy surface were obtained for an immersion time of 24 hours.

In Figure 7a, corresponding to HT-2-MBI (50 ppm), it is observed that a uniform coating was not presented after an immersion time of 24 hours. The chemical analysis shows the presence of chloride ions in the hydrotalcite matrix (Figure 7d). However, in Figure 7b, when the HT-2-MBI (100 ppm) is evaluated, it shows a uniform coating and its chemical analysis does not show the presence of chloride ions (Figure 7e), which is attributed to the fact that there is better protection of the metallic surface. Finally, for HT-2-MBI (200 ppm), there was not a compact coating as a result of its poor corrosion inhibition (Figures 7c and 7f).
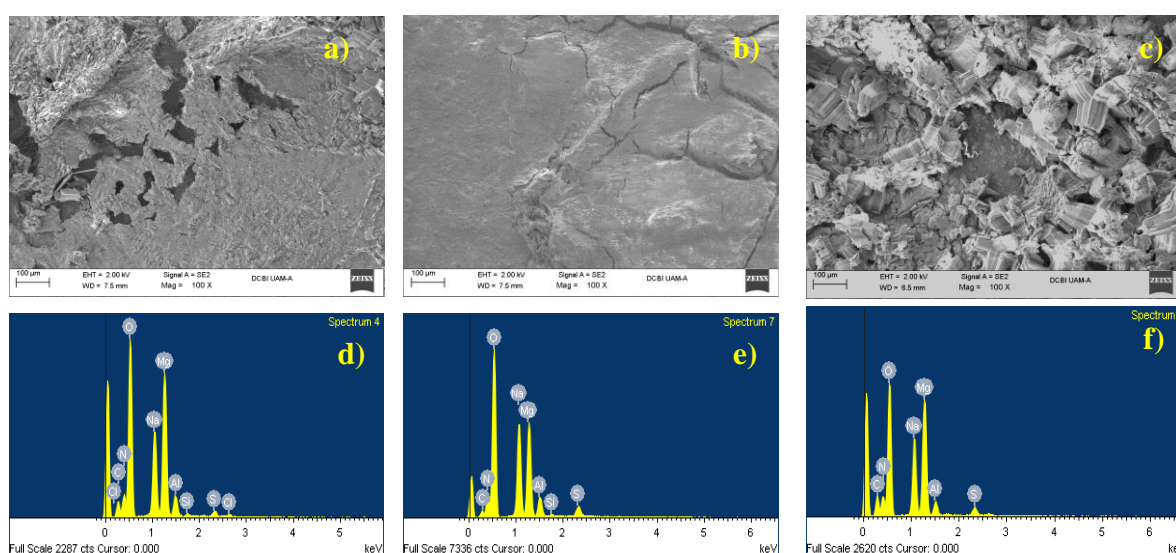

Figure 7. SEM-EDS images of the different concentrations of HT-2-MBI a) and d) 50 ppm, b) and e) 100 ppm and c) with f) 200 ppm

4. CONCLUSIONS

The electrochemical analysis of the AS21 alloy using Hank's solution at 37°C with an HT-2-MBI (100 and 200 ppm) coating demonstrated these conditions as best for protecting the metallic surface from the corrosion process. However, the HT-2-MBI (100 ppm) coating remained for around 102 hours of immersion with $\eta \sim 72\%$.

By means of polarization curves, it was demonstrated that there is a synergic effect with the presence of HT-2-MBI as a corrosion inhibitor as it has a lower current density value.

Finally, it was corroborated with SEM-EDS that the HT-2-MBI (100 ppm) generates the best surface to protect the AS21 alloy.

References

1. A. Imandoust, C. Barrett, T. Al-Samman, K. Inal, H. El Kadiri, *J. Mat. Sci.*, 52 (2017) 1.
2. B. Zberg, P.J. Uggowitzer, J.F. Löffler, *Nat. Mat.*, 8 (2009) 887.
3. W. Xu, N. Birbilis, G. Sha, Y. Wang, J.E. Daniels, Y. Xiao, M. Ferry, *Nat. Mat.*, 14 (2015) 1229.
4. Y. Zhang, J. Xu, Y.C. Ruan, M.K. Yu, M. O'Laughlin, H. Wise, D. Chen, L. Tian, D. Shi, J. Wang, *Nat. Med.*, 22 (2016) 1160.
5. J. Chen, K. Kang, Y. Song, E. Han, S. Ma, J. Ao, *Coatings.*, 9 (2019) 113.
6. C. Liu, Y. Xin, X. Tian, P.K. Chu, *Thin Solid Films.*, 516 (2007) 422.
7. F. Witte, *Acta Biomater.*, 6 (2010) 1680.
8. H. Hornberger, S. Virtanen, A. Boccaccini, *Acta Biomater.*, 8 (2012) 2442.
9. I. Polmear, *Light Alloys.*, (2005) 237.
10. A. Smalenskaite, M.M. Kaba, I. Grigoraviciute, L. Mikoliunaite, A. Zarkov, R. Ramanauskas, I. Morkan, A. Kareiva, *Mater.,* 12 (2019) 3738.
11. L. Wang, K. Zhang, H. He, W. Sun, Q. Zong, G. Liu, *Surf. Coat. Technol.*, 235 (2013) 484.
12. D. Álvarez, A. Collazo, M. Hernández, X. Nóvoa, C. Pérez, *Prog. Org. Coat.*, 68 (2010) 91.
13. L. Wang, Q. Zong, W. Sun, Z. Yang, G. Liu, *Corros. Sci.*, 93 (2015) 256.
14. D.T. Nguyen, H.T.X. To, J. Gervasi, M. Gonon, M. Olivier, *Prog. Org. Coat.*, 124 (2018) 256.
15. D.N. Thuy, H.T.T. Xuan, A. Nicolay, M. Olivier, *Prog. Org. Coat.*, 101 (2016) 331.
16. A. Liu, X. Ju, H. Tian, H. Yang, W. Li, *Appl. Surf. Sci.*, 493 (2019) 239.
17. J. Lin, J. Uan, Formation of Mg, *Corros. Sci.,* 51 (2009) 1181.
18. J. Wang, D. Li, X. Yu, X. Jing, M. Zhang, Z. Jiang, *J. Alloys Compd.*, 494 (2010) 271.
19. Y. Zhao, Y. Chen, W. Wang, Z. Zhou, S. Shi, W. Li, M. Chen, Z. Li, *Mater. Lett.*, (2020) 127349.
20. R. C. Zeng, Z. G. Liu, F. Zhang, S.-Q. Li, H.-Z. Cui, E.-H. Han, *J. Mat. Chem. A*, 2 (2014) 13049.
21. P. Morales, G. Negrón, M. Romero, C. Ángeles, M. Palomar, *Electrochim. Acta.*, 49 (2004) 4733.
22. A. Espinoza, G. Negrón, M. Palomar, M.A. Romero, I. Rodríguez, H. Herrera, *ECS Trans.*, 20 (2009) 543.
23. P. Morales, M. Walczak, C.R. Camargo, R. Cottis, J. Romero, R. Lindsay, *Corros. Sci.*, 101 (2015) 47.
24. W.T. Reichle, *J. Catal.*, 94 (1985) 547.
25. T. Sato, K. Kato, T. Endo, M. Shimada, *React. Solids.*, 2 (1986) 253.
26. A. Luo, M. Pekguleryuz, *J. Mat. Sci.*, 29 (1994) 5259.
27. A. Dehghani, G. Bahlakeh, B. Ramezanzadeh, *Bioelectrochem.*, 130 (2019) 107339.
28. M.A. Bidi, M. Azadi, M. Rassouli, *Mater. Today Commun.*, 24 (2020) 100996.
29. A. Abdel-Gaber, B. Abd-El-Nabey, E. Khamis, D. Abd-El-Khalek, *Desalination.*, 278 (2011) 337.
30. A. Abdel-Gaber, B. Abd-El Nabey, E. Khamis, O. Abdelattef, H. Aglan, A. Ludwick, *Prog. Org. Coat.*, 69 (2010) 402.
31. R.-G. Hu, S. Zhang, J.-F. Bu, C.-J. Lin, G.-L. Song, *Prog. Org. Coat.*, 73 (2012) 129.
32. A. Dermaj, N. Hajjaji, S. Joiret, K. Rahmouni, A. Srhiri, H. Takenouti, V. Vivier, *Electrochim. Acta.,* 52 (2007) 4654.
33. A. Espinoza, F. J. Rodríguez, *RSC Adv.*, 6 (2016) 70226.
34. R. Farahati, S.M. Mousavi, A. Ghaffarinejad, H. Behzadi, *Prog. Org. Coat.*, 142 (2020) 105567.
35. H.O. Ćurković, T. Kosec, K. Marušić, A. Legat, *Electrochim. Acta.*, 83 (2012) 28.

36. E. Alibakhshi, M. Ramezanzadeh, G. Bahlakeh, B. Ramezanzadeh, M. Mahdavian, M. Motamedi, *J. Mol. Liq*., 255 (2018) 185.
37. S. Bender, J. Goellner, A. Heyn, S. Schmigalla, *Mater. Corros.*, 63 (2012) 707